Flame morphology during acceleration in unobstructed channels: effect of fundamental combustion properties

C. Mejía-Botero[a,b], F. Virot[a], L.F. Figueira da Silva[a], J. Melguizo-Gavilanes[a,c]

[a] *Institut Pprime, CNRS, ISAE–ENSMA, Université de Poitiers, BP 40109, 86961 Futuroscope–Chasseneuil Cedex, France*
[b] *Aix Marseille Université, CNRS UMR7342, Centrale Marseille, IRPHE, Marseille, France,*
[c] *Shell Global Solutions B.V., Major Hazards Management, Energy Transition Campus, 1031 HW Amsterdam, The Netherlands*

1 Introduction

Following an accidental ignition of a reactive cloud, a deflagration may be initiated which then expands and accelerates within the process enclosure. Under certain conditions, the accelerated flame can yield a detonation; this is the so-called deflagration-to-detonation transition (DDT). One of the key factors influencing the flame acceleration (FA) in unobstructed channels is flame morphology. It influences the flame surface area, which in turn influences the consumption rate and flame speed. Interestingly, very little work has focused on characterizing the flame and shock morphologies, and no correlation has been suggested between flame morphologies and the fundamental combustion properties (FCP) during the entire DDT process; this is the main objective of this work.

This research is part of an experimental study carried out at the Pprime laboratory [1, 2] in which the effect of FCP on the 3D flame and shock morphologies during the whole DDT process was analyzed using a two-directional schlieren visualization setup. In order to perform a thorough feature selection analysis, we compiled a database of morphologies from the literature, in which we considered papers that reported similar characteristics to those obtained in our experiments. The study focuses only on unobstructed channels where ignition is effected at a closed side of the channel. The FCP considered are the expansion ratio (σ), laminar flame speed (s_L), laminar flame thickness (δ_f), Zel'dovich number (β), effective Lewis number (Le_eff), deficient reactant Lewis number (Le_D), heat capacity ratio (γ), and sound speed relative to the combustion products (c_b) [3]. Logistic regression techniques are used to propose FCP boundaries to determine the properties that affect the flame morphology during the DDT. These boundaries can serve as guidelines for the study of specific flame morphologies during acceleration in unobstructed channels. Additionally, they enable to pinpoint the experimental conditions for which few data are reported in the literature, thus suggesting future research directions on this topic.

2 Flame and shock morphology types and database information

During the study carried out in [1], different experimental campaigns were designed to compare the morphologies for a wide range of FCP. In total, nine (9) mixtures were assessed: (i) $2H_2 + O_2 + N_2$, (ii) $2H_2 + O_2 + 2.8Ar$, (iii) $2H_2 + O_2 + 2.8He$, (iv) $2H_2 + O_2 + 1.5Ar + 1.3He$, (v) $2H_2 + 1.25O_2$, (vi) $2H_2 + 0.58O_2$, (vii) $0.8H_2 + 0.2CH_4 + 0.8O_2$, (viii) $0.5H_2 + 0.5CH_4 + 1.25O_2$, and (ix) $CH_4 + 2O_2$. Two

Correspondence to: cristian-camilo.mejia-botero@ensma.fr

characteristic flame morphologies evolutions were systematically observed during the FA. Figure 1 (a) shows the first one, for which after the formation of a finger shape flame (image 1), the flame inverts (images $2-7$) taking the characteristic tulip flame shape, which is labeled in this work as the *early stage* 1 (ES1) morphology. After this, the flame becomes asymmetric (images $8-9$) and when the precursor shock wave is formed, a relatively short flame with the tip centered in the channel is observed, called the *late stage* 1 (LS1) morphology. The transition ES1 $\rightarrow$ LS1 was systematically observed for the mixtures (ii), (iii), and (iv). Figure 1 (b) shows the second morphology type. In this case, after the finger shape flame (image 1), the flame is wrinkled (images $2-6$) yielding an elongated flame that is labeled as *early stage* 2 (ES2) morphology. After this, an asymmetric flame is observed (image 7) and during the formation of the precursor wave, a long flame, with the tip inclined to a corner (image 8), is observed, which is called here the *late stage* 2 (LS2) morphology. The transition ES2 $\rightarrow$ LS2 was systematically observed for the mixtures (v), (vii), (viii), and (ix). Surprisingly, the mixtures (i) and (vi) showed the ES1 $\rightarrow$ LS2 transition, which means that during the early stages of FA, the tulip flame was observed, but during the late stages a long flame with the tip inclined to a corner is produced during the precursor wave formation.

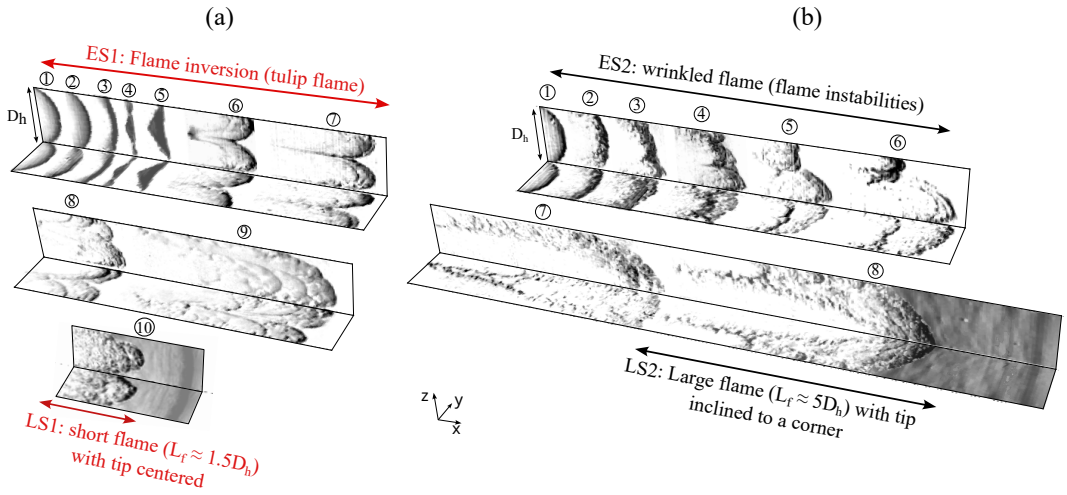

Figure 1: Characteristic flame morphology during flame acceleration (FA), (a) ES1 $\rightarrow$ LS1, and (b) ES2 $\rightarrow$ LS2 transition.

The evolution observed during our experiments have been also obtained in different works in the literature. This allowed us to compile a morphology database to extend the range of experimental conditions to be analyzed. In total, 60 data points were collected [1], which were obtained in channels with closed-closed and closed-open ends, with the ignition at one of the closed ends. Furthermore, channels with circular and squared cross sections are considered, which shows that the flame morphology does not seem to be geometry-dependent under the conditions studied. Our data points and those collected from the literature comprise H_2, CH_4, CH_4/H_2 blends, C_2H_2, C_2H_4, and C_3H_8. The oxidizer is O_2 for all the data points, and some mixtures are diluted with N_2, Ar, or He. All the tests were performed at room temperature, i.e., $T \approx 300$ K. The range of conditions considered are hydraulic diameter $D_\mathrm{h} \in [10, 100]$ mm, channel length $L \in [0.15, 6]$ m, and equivalence ratio $\phi \in [0.42, 7.13]$. Expectedly, all tests under the closed-open configuration were performed at atmospheric pressure ($p \approx 1$ bar). However, several of the tests with the closed-closed configuration were carried out below/above atmospheric pressure, i.e., $p \in [0.08, 1.5]$ bar. Not all the works in the literature reported the morphologies during all stages of FA. In fact, most of them only report morphologies during the early stages, whereas other do so during the late stages only. For this reason, the ES and LS data are analyzed separately: 53 data points that

[1] All references are included in [1], and not listed here due to space limitations.

reported ES are used to map the flame morphologies as a function of FCP pairs, and thereby observe if a clear separation exists between the morphologies identified. The remaining seven (7) data points that reported morphologies during LS only are used as a test dataset to assess the validity of the proposed boundaries.

3 Early stages analysis: FCP boundaries proposal

3.1 Feature selection methodology

The methodology used to determine which are the FCP that most affect flame morphology is the Recursive Feature Elimination (RFE) technique, available in scikit-learn package [4], which objective is to select the most important features by recursively considering smaller sets of features. As the dependent variables are categorical, i.e., ES1 or ES2 morphologies, it is necessary to binarize them. We assign the value of 0 to ES1 and 1 to ES2. Furthermore, since the FCP considered, used as independent (or predictor) variables have significantly different scales, these are normalized to ensure that the features are statistically distributed on a common scale, thus improving the model performance. Subsequently, the Logistic Regression Model (LRM) [5] is used to classify the morphologies. Accordingly, the algorithm uses the experimental data to maximize the probabilities of obtaining 0 or 1, i.e., ES1 or ES2, using the maximum likelihood estimator [6].

Lastly, it is necessary to choose a scoring metric, with which the model performance is evaluated. Here, the $F1$ score is used, which can be interpreted as a harmonic mean of the model accuracy, being 1 its best score, and 0 its worst,

$$F1 = \frac{2 \times TP}{2 \times TP + FP + FN}, \tag{1}$$

where TP is the number of true positive values, i.e., those that are well predicted by the model, FN the number of false negative values, and FP the number of false positive values. A FP is an error in which a test result incorrectly indicates the presence of a condition, whereas a FN is the opposite error, where the test result incorrectly indicates the absence of a condition when it is present. Thus, $FP + FN$ is the number of values that are wrongly predicted by the model. With these methodological steps, the RFE systematically evaluates the performance of the model using the chosen FCP. The RFE starts by computing the model using each FCP as an independent variable, and reporting the associated average $F1$ score. Then, it repeats this evaluation, but using all the possible pairs of FCP as independent variables, determining the average of the $F1$ scores obtained. This step is repeated systematically by evaluating the model with $3, 4, ..., n$ FCP as independent variables, where n denotes the number of FCP selected. For this analysis, $n = 8$, i.e., $n \in \{\sigma, \sigma s_\mathrm{L}/c_\mathrm{b}, \delta_\mathrm{f}, D_\mathrm{h}/\delta_\mathrm{f}, \beta, \gamma, Le_\mathrm{eff}, Le_\mathrm{D}\}$.

3.2 Most important pairs of FCP for flame morphology estimation

The RFE analysis (Figure 2 (a)) shows that there is not a $F1$ score improvement when using more than two (2) FCP in the LRM, thus the analysis is focused on FCP pairs only. To determine which is the best FCP combination, the auto-$F1$ score matrix is used (Figure 2 (b)), which shows the $F1$ score given the pairs of FCP. The main diagonal values indicate the score using only a single FCP in the predictive model. Figure 2 (b) shows that the pairs involving σ always have the highest $F1$ scores. Note that the $F1$ score with σ alone ($F1 = 0.94$) is the same as that using σ with δ_f, $D_\mathrm{h}/\delta_\mathrm{f}$, β, γ and Le_D. It is thus clear that σ is the parameter that the most influences the morphology changes during the early stages, under the conditions studied. The $F1$ score is maximum for the pairs $(\sigma, \sigma s_\mathrm{L}/c_\mathrm{b})$ and $(\sigma s_\mathrm{L}/c_\mathrm{b}, \gamma)$, with $F1 = 0.98$, which also underscores the importance of these properties on the development of

the flame morphology during the early stages of FA. The other pairs that present a large $F1$ score are $(\sigma s_L/c_b, Le_{eff})$, with $F1 = 0.94$, and $(\sigma s_L/c_b, Le_D)$ with $F1 = 0.94$. Considering only the effect of individual FCP, the best scores are consistently obtained for σ and $\sigma s_L/c_b$, but the γ score is not negligible ($F1 = 0.81$). The latter suggests that γ should affect the flame morphology, but it appears to be less important than either σ or $\sigma s_L/c_b$.

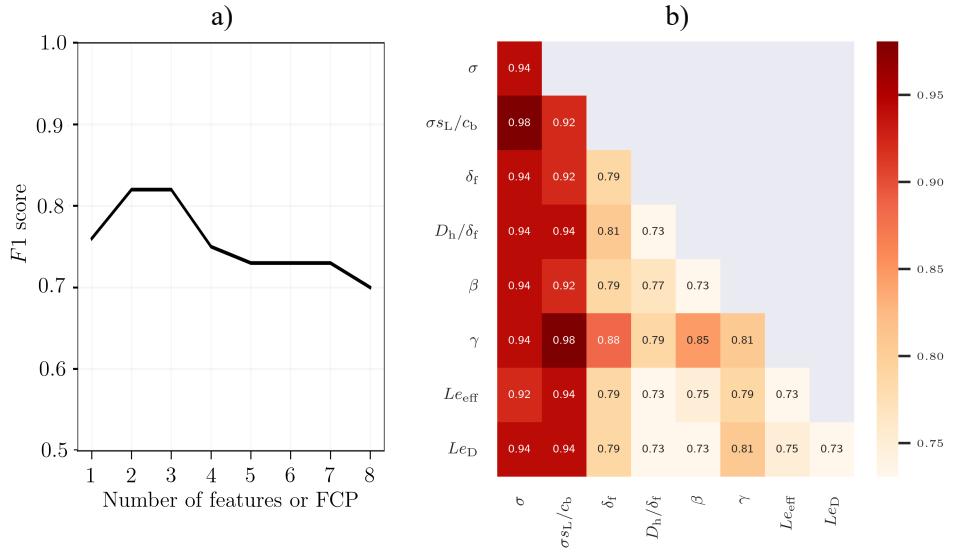

Figure 2: Recursive Feature Elimination results with Logistic Regression (a) Average $F1$ score, and (b) auto-$F1$ score matrix, where each number represent the test accuracy for the respective pair of FCP. The main diagonal corresponds to the $F1$ score using a single FCP only.

3.3 Optimal flame morphology boundaries

As determinated above, the FCP pairs that best separate the morphologies during the early stages are $(\sigma s_L/c_b, \sigma)$, and $(\gamma, \sigma s_L/c_b)$. Accordingly, the optimal boundaries obtained using the LRM for these pairs are presented in Figure 3. Note that data that report morphologies during the entire FA process i.e., ES1 $\rightarrow$ LS1, ES2 $\rightarrow$ LS2, and ES1 $\rightarrow$ LS2, as well as data that only report morphologies during the early stages, i.e., ES1 or ES2, are painted with different colors. In the case of the pair $(\sigma s_L/c_b, \sigma)$, the ES1 morphology region lies below and the ES2 above the boundary line, whereas for $(\gamma, \sigma s_L/c_b)$, ES2 morphologies are found below, and ES1 above the boundary line. The condition to obtain the ES1 morphology using the first pair is $\sigma s_L/c_b < -0.0095\sigma + 0.13$, and using the second pair is $\gamma > 2.2\sigma s_L/c_b + 1.3$.

The boundaries proposed can almost completely separate the morphology ES1 and ES2, coherently with the high $F1$ scored obtained with these pairs. Also, note that the two points that yield the ES1 $\rightarrow$ LS2 transition have almost the same $\sigma s_L/c_b$, and are close to the boundary, which suggest that these mixtures are in a morphology transition stage. In addition, when analyzing H_2 and hydrocarbon (HC) mixtures separately, it can be observed that both fuel mixtures exhibit a similar trend but with a different slope. However, note that there is a black point around $\sigma \approx 6$ that exhibits the ES2 but it is not well predicted by the model for any of the evaluated pairs of FCP, since it lies in the ES1 (red) region. This point corresponds to the leanest H_2 mixture reported in the database ($\phi = 0.42$), it may thus be affected by thermo-diffusive instabilities. This explains why, in spite of having a low $\sigma s_L/c_b$ and σ, which is characteristic of the ES1 morphology, it presented a wrinkled flame (ES2). This last result suggests that

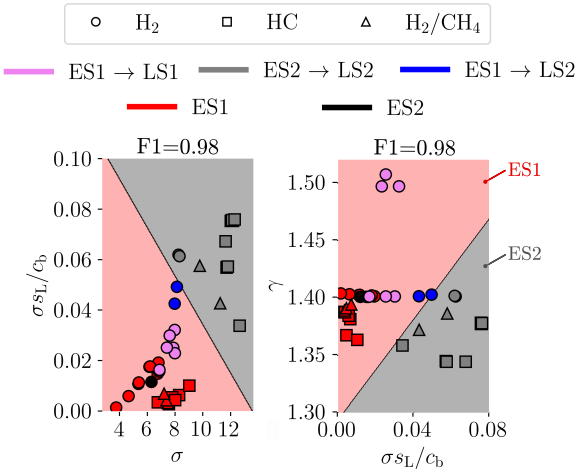

Figure 3: Optimal boundaries between the ES1 an ES2 morphology types, determined with the the Logistic Regression Model for the pairs of FCP that yield better $F1$-scores. Line equations are $\sigma s_L/c_b = -0.0095\sigma + 0.13$, and $\gamma = 2.2\sigma s_L/c_b + 1.3$.

the proposed boundaries could not be able to predict flame morphologies that exhibit thermo-diffusive instabilities. Experimental data under ultra-rich and ultra-lean conditions are needed to further improve the FCP boundaries, in particular to account for the effect of thermo-diffusive instabilities.

4 Late stages analysis: FCP boundaries testing

As shown in Figure 4, the boundaries proposed using the ES data are used to test seven (7) data points that reported LS2 morphology only. Note that the graph appears to report only five (5) points, which is due to two superimposed pairs that were developed under similar experimental conditions. In addition, the points reporting ES $\rightarrow$ LS transitions are not considered in this analysis, as they were already used to determine the morphology boundaries. For ($\sigma s_L/c_b$, σ) it is seen that all the hydrocarbons (HC), that have higher σ values compared to the H_2 mixtures, are correctly predicted by all the boundaries. On the other hand, for the two H_2 mixtures considered, this boundary is not predictive for ($\sigma s_L/c_b \approx 0.04$, $\sigma \approx 7.5$). This corresponds to a lean mixture of H_2/O_2, at $p = 10$ kPa and $\phi = 0.5$. This condition is not predicted by the pair (γ, $\sigma s_L/c_b$) either, and the flame surface evolution may be influenced by thermo-diffusive instabilities, which, as previously discussed, are not expected to be captured by the proposed boundaries. This analysis shows that the FCP pairs observed to govern the flame morphologies at ES seem to hold with the LS data, suggesting a strong correlation between both the early and late stages of FA. Finally, these boundaries also worked well for different detonation onset (DO) cases observed in the experiments [1], which suggest a correlation between the morphology during the flame acceleration process and the DO mechanisms.

5 Conclusions

The flame morphologies observed during the early and late stages of the flame acceleration process in unobstructed channels were analyzed using experimental images. Boundaries were proposed using two characteristic morphology evolutions observed during the early stages, i.e., ES1 and ES2, together with recursive feature elimination, and logistic regression techniques. Results showed that the fundamental combustion properties pairs that are capable of separating the flame morphology evolutions at this stage

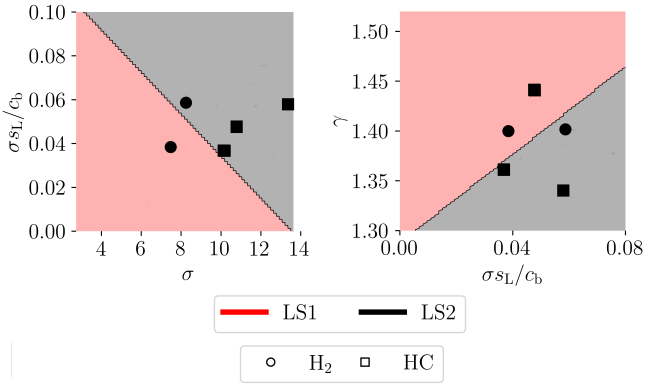

Figure 4: Optimal boundary testing with the LS data that only reported morphology at the LS.

are $(\sigma, \sigma s_L/c_b)$, and $(\sigma s_L/c_b, \gamma)$. In order to evaluate any relationship between the early and late stages, the boundaries proposed using the early stages data were tested against the late stages, showing that the fundamental combustion properties that can describe the morphologies during early stages can also do so during later ones. With these boundaries, it was also demostrated that (i) the two mixtures that showed the ES1 $\rightarrow$ LS2 morphology are in a morphology transition state, evidenced by the proximity of these mixtures to the proposed boundaries, and (ii) lean H_2 mixtures are wrongly predicted. Finally, this work provides a map of flame morphologies as a function of the fundamental combustion properties which can serve as guide for future research focusing/targeting specific morphological features.

Acknowledgements

The authors gratefully acknowledge the financial support from *l'Agence Nationale de la Recherche* Program JCJC (FASTD ANR-20-CE05-0011-01), l'école doctorale MIMME, and FM Global.

References

[1] C. Mejia-Botero. *Flame and shock morphologies and dynamics during acceleration and transition to detonation in unobstructed channels: effect of fundamental combustion properties*. PhD thesis, ISAE-ENSMA Ecole Nationale Supérieure de Mécanique et d'Aérotechique, 2024.

[2] C. Mejia-Botero, F. Virot, and J. Melguizo-Gavilanes. CH_4-O_2 flame acceleration morphology: A comparative analysis under different hydrocarbon fuel, channel geometry and scale. *ICDERS*, 2023.

[3] C Mejía-Botero, F Virot, LF da Silva, and J Melguizo-Gavilanes. A detonation run-up distance database: Data-driven existing models improvement and new model development. *Proceedings of the Combustion Institute*, 40(1-4):105444, 2024.

[4] F. Pedregosa, G. Varoquaux, A. Gramfort, V. Michel, B. Thirion, O. Grisel, M. Blondel, P. Prettenhofer, R. Weiss, V. Dubourg, J. Vanderplas, A. Passos, D. Cournapeau, M. Brucher, M. Perrot, and E. Duchesnay. Scikit-learn: Machine learning in Python. *Journal of Machine Learning Research*, 12:2825–2830, 2011.

[5] D. Cox. The regression analysis of binary sequences. *Journal of the Royal Statistical Society: Series B (Methodological)*, 20(2):215–232, 1958.

[6] J. Pfanzagl. *Parametric statistical theory*. Walter de Gruyter, 2011.